Research Article

Effects of annealing and firing in wet hydrogen on the dielectric breakdown strengths of alumina ceramics

Jishi DU[a,*], Binghua TANG[a], Wei LIU[a], Tao ZHANG[a,b],
Jiagen PENG[a], Hu CHEN[a], Yangjun LEI[a]

[a]*Institute of Electronic Engineering, China Academy of Engineering Physics, Mianyang 621900, China*
[b]*Department of Materials Science, Sichuan University, Chengdu 610064, China*

Abstract: Annealing and firing in wet hydrogen are widely used steps in the processing alumina–ceramic insulators that may affect their dielectric breakdown strengths (DBS). In this study, the effects of annealing (at 1300 ℃ for 7 h) and firing in wet hydrogen on the DBS of alumina ceramics (all sintered at 1650 ℃) were studied, and the underlying mechanisms were analyzed by material characterizations. Annealing reduced the DBS of the 95% alumina ceramics due to the inter-granular phase crystallization, and the reduction in the DBS could be correlated to the reduction in mechanical strength. In contrast, annealing improved the DBS of the 99% alumina ceramic without intergranular phase transformation. Firing in wet hydrogen at 1500 ℃ caused the DBS increment, which can be ascribed to the reduction in the concentrations of point defects and electrical carriers.

Keywords: alumina ceramic; dielectric breakdown strength (DBS); inter-granular phase crystallization; firing in wet hydrogen

1 Introduction

The alumina ceramics are commonly used as insulation materials, mainly because of their low prices, capacity to be easily shaped, high flexural strengths, good stability at high temperatures, low dielectric loss, and their high dielectric breakdown strengths (DBS). Annealing and firing in wet hydrogen are widely carried out in processing alumina–ceramic insulators. For example, alumina–ceramic insulators are always required to be annealed at a temperature lower than the sintering temperature to burn away any possible contaminations on their surfaces and diminish the residual stress introduced by the grinding. The alumina–ceramic insulators are heated in wet hydrogen at a high temperature when sealed with the metal electrodes [1]. Annealing and firing in wet hydrogen may induce some reactions in alumina ceramics, which may affect the DBS.

Annealing could induce an inter-granular phase transformation in alumina ceramics. Chemical impurities in raw alumina powders cannot be eliminated, and some chemical impurities are intentionally added in order to optimize the performances of alumina ceramics and promote sintering. Some of the chemical impurities have very low solubilities in the alumina lattice. Park and Yoon [2] found that the solubility limit of Ca in the alumina lattice was only about 20 ppm, while the solubility limit of Si in the alumina lattice was several

* Corresponding author.
E-mail: flash6669@163.com

hundreds of ppm. The excessive chemical impurities always segregate at the grain boundaries, and sometimes exist in the form of liquid phases during sintering [3,4]. Powell-Dogan *et al*. [5–7] reported that most of the sintering aids (MgO, SiO_2, CaO) were present at the grain boundaries as continuous amorphous or glassy phases in a 96% alumina ceramic, and that the inter-granular amorphous phases would crystallize when the alumina ceramic was annealed at a relatively modest temperature. The inter-granular phase crystallization induced by annealing may change the DBS of alumina ceramics. Liebault *et al.* [8] reported that annealing at 1200 ℃ improved the DBS of two alumina ceramics with 5%–8% sintering aids, and they reasoned that the crystalline phases developed on the surface were more able to trap electrical carriers to prohibit the dielectric breakdown (DB). However, though Touzin *et al*. [9] argued that a high content of crystalline anorthite did not favor the DBS of alumina ceramics at room temperature, they did not provide any evidence to support their argument. As no more reports on the effect of inter-granular phase crystallization on the DBS of alumina ceramics were found, this issue remains controversial.

When the alumina ceramics are processed in a different atmosphere, their electrical conductivities can change due to the varying concentrations of point defects. Pappis and kingery [10] found that the electrical conductivity of alumina increased at both high and low oxygen pressures, and they reasoned that the concentrations of electrical carriers changed with the oxygen pressure as a result of the changing concentrations of point defects. Miranzo *et al*. [11] reported that sintering in a CO/CO_2 atmosphere improved the electrical conductivity of an alumina ceramic at 600 ℃ by five orders of magnitude. The DB and surface flashover were both correlated to the transport of electrical carriers [12]. Jaitly *et al*. [13] reported that firing in wet hydrogen reduced the surface flashover voltages of alumina ceramics, and improved the surface electrical resistances. However, the effect of firing in wet hydrogen on the DBS of alumina ceramics has not been reported.

In this study, two 95% SiO_2–CaO co-doped alumina ceramics were sintered, and then quenched to keep the inter-granular phases amorphous. Annealing was performed at a modest temperature for a long time to induce the crystallization of the amorphous inter-granular phases. The DBS was measured before and after annealing. For comparison, a 99% alumina ceramic

was treated in the same way and the effect of annealing on the DBS without inter-granular phase transformation was analyzed. The aforementioned three alumina ceramics were all heated in wet hydrogen at a high temperature for a short time to investigate the effect of firing in wet hydrogen on the DBS of alumina ceramics. Densities, the roughness of the surfaces, reflectance spectra, crystalline phases, bending strengths, surface and fracture microstructures, chemical compositions, electrical conductivities, dielectric constants, and losses of the samples before and after treatments were characterized to study the mechanisms behind the effects.

2 Experimental

2.1 Sample preparation

Three alumina ceramics were named as "A95", "B95", and "A99". The chemical composition of A95 was: 94.7 wt% Al_2O_3, 2.62 wt% SiO_2, 2.16 wt% CaO, 0.08 wt% MgO, 0.09 wt% Na_2O, and 0.05 wt% Fe_2O_3. A99 contained more than 99 wt% Al_2O_3 with a little Y_2O_3. A95 and A99 sheets with a diameter of 30 mm were shaped by dry pressing in a tungsten–steel die with an axial pressure of 100 MPa, and then repressed by cold-isostatic pressing at 170 MPa. The chemical composition of B95 was: 94.5 wt% Al_2O_3, 2.2 wt% SiO_2, and 3.3 wt% CaO. Sheets of B95 with a diameter of 40 mm were prepared by the low-pressure injection molding technique and the partial wick-debinding technique [14,15].

The green bodies were sintered in a muffle furnace heated by $MoSi_2$ in air following the sintering temperature curve shown in Fig. 1. During the sintering, all the sheets were placed on the sintered 99% alumina plates, on which some 60 mesh corundum powder was sprinkled. The thicknesses of the as-sintered A99, A95, and B95 sheets were 2.51, 2.37, and 3.61 mm, respectively, and the diameters of the as-sintered A99, A95, and B95 sheets were about 25, 26, and 36 mm, respectively. All the as-sintered sheets were polished in vibrating alumina ceramic shivers at 1500 Hz for 1 h. The B95 sheets were machined into 1.98 mm-thick sheets by grinding both surfaces using a grind wheel of 400 mesh diamond.

After sintering, the temperature dropped to about 1250 ℃ within 1 h, so it was believed that the liquid
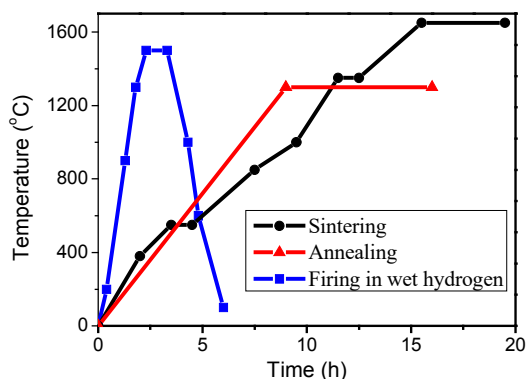
Fig. 1 Sintering temperature curve, the annealing temperature curve, and the temperature curve of firing in wet hydrogen.

phases in A95 and B95 during sintering were frozen into certain types of amorphous inter-granular phases. After sintering and polishing, five additional processes were carried out: surface grinding, annealing, firing in wet hydrogen, polishing, and quenching. Annealing was conducted in a muffle furnace heated by $MoSi_2$ in air following the temperature curve in Fig. 1. Firing in wet hydrogen was conducted in a molybdenum-heating oven following the temperature curve in Fig. 1, and when the temperature was lower than 900 ℃, nitrogen was pumped into the oven, while wet hydrogen with a dew point of 30 ℃ was pumped into the oven when the temperature was higher than 900 ℃. Some of the annealed A99 sheets were polished by the aforementioned method for 2 h in order to analyze the effect of polishing on the DBS. A few of the annealed B95 samples were heated to 1650 ℃ at a rate of 150 ℃/h, maintained at 1650 ℃ for 10 min, and then quenched to 1250 ℃ within 1 h in order to analyze the change in DBS when the inter-granular phase crystallization was eliminated. All the processed samples were washed in deionized water for 1 h by a supersonic washer, and then dried at 100 ℃ in a drying oven for 24 h. The samples are identified by the names of the alumina ceramics and the order in which the additional processes used in their preparation were carried out. For example, "B95-G-A-Q" is the name of the B95 sheets that were processed by surface grinding, annealing, and quenching, in that order. In the naming convention that was followed, "G", "A", "FWH", "P", and "Q" are abbreviations for surface grinding, annealing, firing in wet hydrogen, polishing, and quenching, respectively.

The main properties of the raw materials and more information on the sample preparation can be found in the Electronic Supplementary Material (ESM).

2. 2 Dielectric breakdown test and material characterizations

The DB test was conducted at room temperature. A spherical-to-planar electrode set-up was used. The spherical electrode was a stainless steel ball with a diameter of 4.00 ± 0.005 mm. The planar electrode was a brass cylinder with a diameter of 4 mm that had a fillet with a radius of 0.5 mm at the rim. More details about the electrode set-up can be found in the ESM. During the DB test, the electrode set-up and the sample were immersed in insulation oil to avoid the surface flashover. Before use, the insulation oil was cleaned, degassed, and dried. An AC high voltage power supply of 50 Hz was used in the DB test, and the ramp rate was 1 kV/s. The DB voltage V_b was determined by measuring the abrupt increase in the current, following the specifications of ASTM Standard D149-97a [16]. The occurrence of a DB was accompanied by a sparkle and an explosion. The nominal DBS E_b (DBS for short in this paper) was calculated as: $E_b = V_b/t$, where t was the thickness of the sample (mm). For each condition, five sheets were used to measure the DBS, and four points on each sheet were selected for the measurement. After each DB test, the stainless steel ball was rolled a little to ensure that its surface in contact with the sample was fresh. Each stainless steel ball was used as the spherical electrode 20 times, and no influence of the use time on the measured values was found. It is worth mentioning that it is hard to get the real electric field strength when the DB of the alumina ceramic occurred by the simulation methods, because the DB of the insulation oil occurred prior to the DB of the alumina ceramics; this changed the dielectric constant and the distribution of space charges. More discussions on the DB test can be found in the ESM.

The volume densities were measured using the Archimedes method in water at room temperature. Surface roughness (Sz) was measured by a measuring laser microscope. The crystalline phases were analyzed by X-ray diffraction (XRD, Cu Kα). Surface and fracture microstructures were examined by scanning electron microscope (SEM, back scattered electron), and the chemical compositions at certain points were analyzed by an energy dispersive spectrometer (EDS). A three-point method was used to measure the bending strengths of B95 samples, and the experimental procedure can be found in the ESM. Reflectance spectra of the wavelengths in the range of 200–2500 nm were measured using a UV–Vis–R spectrometer with an

integrating sphere. The frequency dependence of the dielectric constant and the dielectric loss was tested using a precision impedance analyzer from 1 kHz to 2 MHz at room temperature, and gold coatings of diameter 13 mm were sputtered onto the samples. Chemical compositions of some samples were analyzed by X-ray photoelectron spectroscopy (XPS). The DC electrical conductivities at 3 kV were measured, and more details about these measurements can be found in the ESM.

3 Results and discussion

3. 1 Dielectric breakdown strengths of all the samples

Figure 2 displays the measured DBS data sorted in ascending order and their Weibull distribution fitting. Annealing improved the DBS of the 99% alumina as shown in Fig. 2(a), while it reduced the DBS of 95% alumina ceramics, as shown in Figs. 2(b) and 2(c). Quenching improved the DBS of B95-G-A to a higher

level that was even higher than the DBS of B95-G, as shown in Fig. 2(c). Firing in wet hydrogen improved the DBS of alumina ceramics. For the ground samples, A99-G had the highest DBS compared to A95-G and B95-G, as shown in Figs. 2(c) and 2(d). Polishing did not reduce the average DBS of A99-A, but it increased the standard deviation as shown in Fig. 2(a). It should be mentioned that the measured DBS data of the 95% alumina ceramics after annealing could not be well fitted to the Weibull distribution, as shown in Figs. 2(b) and 2(c), and this was different from the previous reports, in which the DBS data could be fitted to the Weibull distribution well [17,18]. Although it seems that the large values of the data of A95-A and B95-G-A damage the fitting to the Weibull distribution, the remaining data cannot be fitted to the Weibull distribution well if the large values are excluded. Although much research work has been done on the distribution of the DBS data, what influences the distribution of the DBS data of alumina ceramics is still unclear.

Annealing and firing in wet hydrogen had almost no
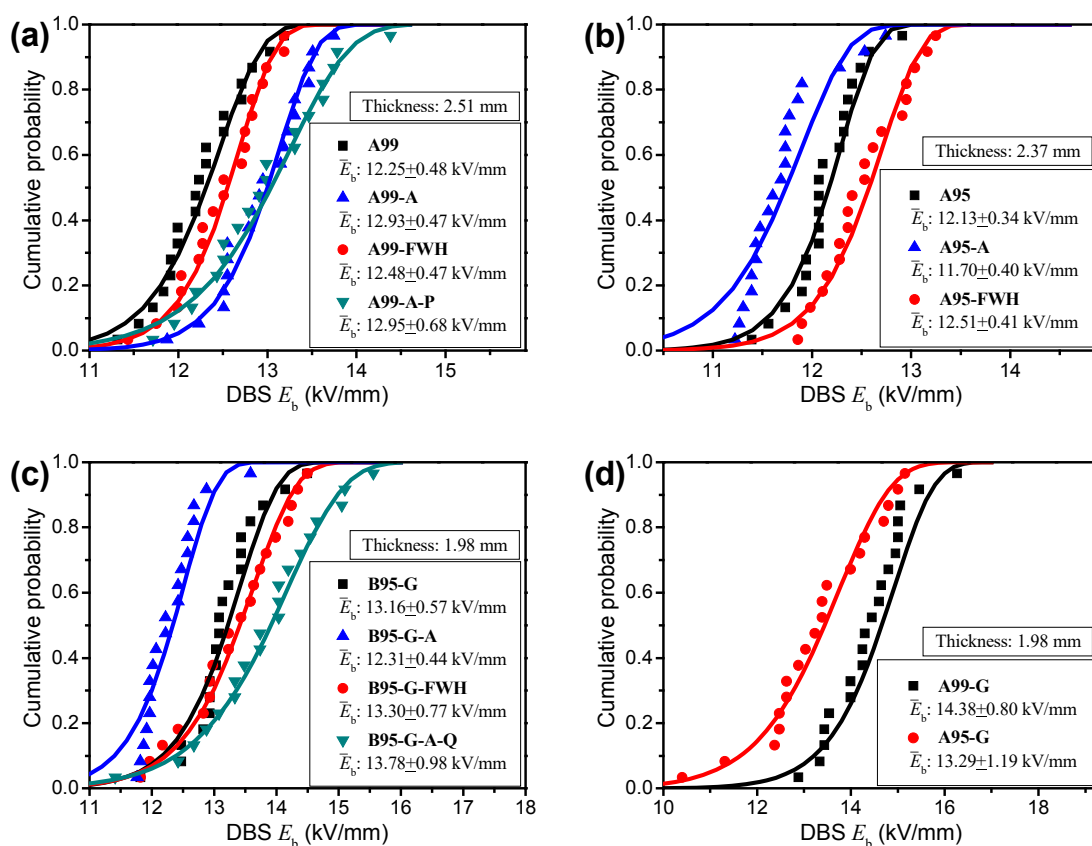
Fig. 2 Measured DBS E_b data sorted in ascending order and the Weibull distribution fitting (lines): the cumulative probability corresponding to the *i*-th value sorted in ascending order is equal to $(i - 0.3)/(n + 0.4)$, where *n* is the total number of the values. The inset data $\bar{E}_b$ is the average value of E_b with the standard deviation.

effects on the densities (Table 1). Therefore, the effects of annealing and firing in wet hydrogen on the DBS of alumina ceramics could not be ascribed to the effects on the densities. No evident relationship between *Sz* (ESM) and the DBS was found. The effects of annealing and firing in wet hydrogen on the DBS of the three alumina ceramics were also not attributed to the effects on the dielectric constants and losses (ESM).

3. 2   Analyses of the underlying mechanisms behind the effects of annealing

Annealing had no effects on the phases of A99, while it made the glassy phase in the 95% alumina ceramics crystallize into gehlenite ($2CaO \cdot 3SiO_2 \cdot 2Al_2O_3$) and anorthite ($CaO \cdot 2SiO_2 \cdot 2Al_2O_3$). Quenching diminished the inter-granular phase crystallization, as shown by the XRD patterns in Fig. 3. Our results were consistent with the results from the work completed by Powell-Dogan *et al*. [5–7]. The inter-granular crystalline phases in 95% alumina ceramics were flake-like and rich in Si and Ca that were eliminated by the quenching, as shown by the SEM images and EDS results in Fig. 4. It should be mentioned that Si and Ca existed on the surface of A95 and B95-G-A-Q, although there were no flake-like structures on the surface of annealed 95% alumina ceramics. The existence of Si and Ca on the

Table 1   Densities of the alumina ceramics before and after treatments (g/cm^3)

Sample \ Condition	As-sintered	Annealed	Fired in wet hydrogen
A99	3.921 ± 0.038	3.919 ± 0.042	3.926 ± 0.029
A95	3.714 ± 0.084	3.711 ± 0.053	3.715 ± 0.075
B95-G	3.668 ± 0.047	3.663 ± 0.039	3.665 ± 0.051

Fig. 3 XRD patterns of 95% alumina ceramics before and after annealing and quenching.
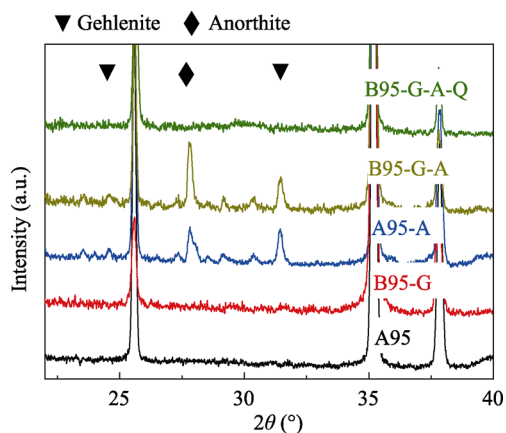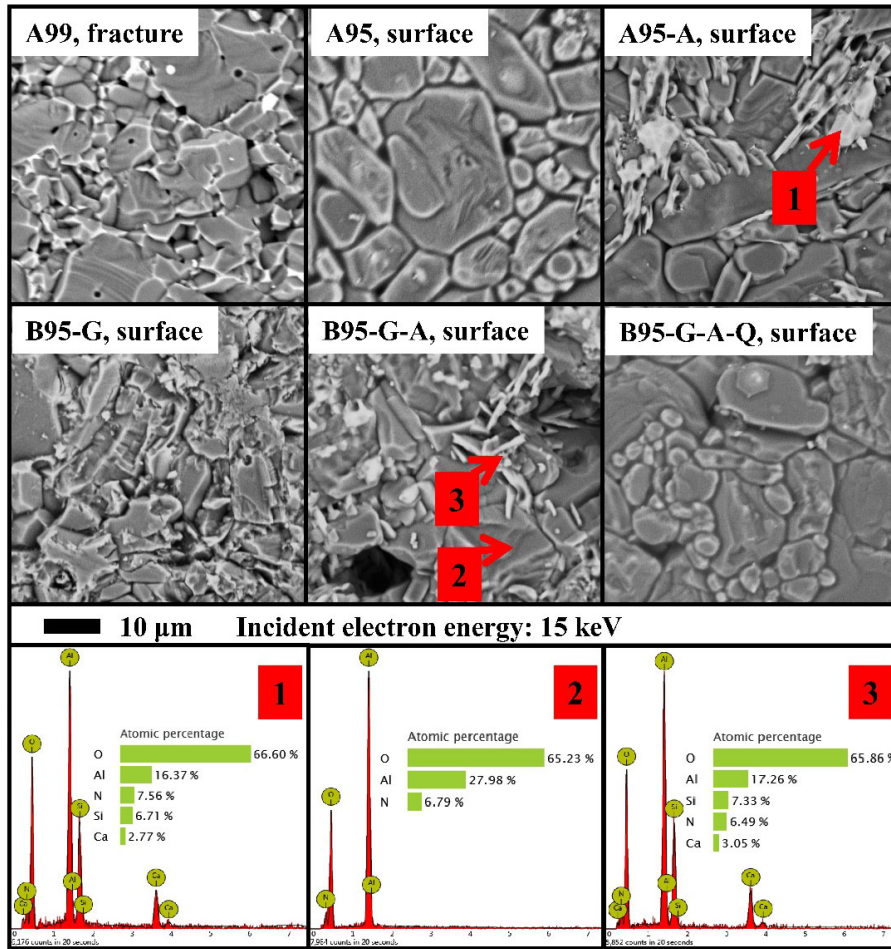
surfaces of A95 and B95-G-A-Q was proven by the XPS spectra shown in Fig. 5, in which, the peaks corresponding to Si and Ca could be detected. Considering that the detection depth of XPS is only several nanometers, it can be concluded that Si and Ca always existed on the surface of the 95% alumina ceramics before and after annealing and quenching. Surface grinding crushed the grains on the surface, and the fragments on the surface coarsened into small grains, as shown in Fig. 4. XRD and EDS showed that the bright spots in A99 were yttrogarnet ($Y_3Al_5O_{12}$) (ESM). Firing in wet hydrogen had no effects on the phases and the microstructures of all the three alumina ceramics except for the slight healing of the ground surface of B95-G. More XRD patterns and SEM images are shown in the ESM.

Comparing the results in Figs. 2–4, it can be concluded that it might be the inter-granular phase crystallization that reduced the DBS of the 95% alumina ceramics after annealing, and hence it is better to avoid the inter-granular phase crystallization when the alumina–ceramic insulators are annealed. The result in this study was consistent with the results from the work of Touzin *et al*. [9] which argued that an alumina ceramic with more crystalline inter-granular phases had a lower DBS than the alumina ceramic with more glassy inter-granular phases. The result in this study contradicted Ref. [8]. Liebault *et al*. [8] did not analyze the phases in those two alumina ceramics before and after annealing; therefore, whether inter-granular phase crystallization had occurred in their experiment is unclear. Further, it was not appropriate to state that inter-granular phase crystallization improved the DBS of the alumina ceramics.

The model of DB based on mechanical properties [19,20] is capable of explaining why the inter-granular phase crystallization decreased the DBS of the 95% alumina ceramics. The inter-granular phase crystallization in alumina ceramics was found to result in a remarkable improvement in the toughness and to lessen the mechanical strengths [21,22]. Tomaszewski [21] attributed the reduction to the micro-cracks generated by the mismatch between the alumina matrix and the crystalline inter-granular phases. Jouini *et al*. [23] found that the microcracks induced by pre-stress led to a reduction in the DBS of an alumina ceramic. Annealing decreased the bending strength of B95, while the quenching which followed annealing recaptured the bending strength, as shown in Fig. 6. The micro-cracks generated by the inter-granular phase crystallization

Fig. 4 SEM (back scattered electron) images: the chemical compositions at three points were analyzed by EDS.
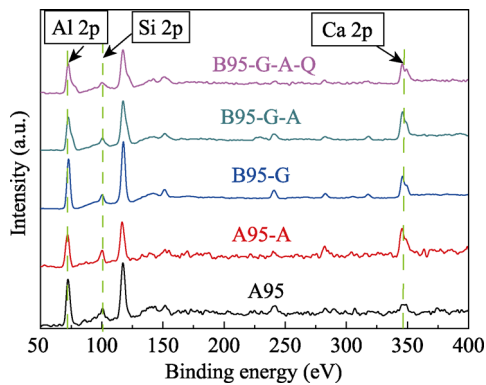

Fig. 5 XPS spectra of the 95% alumina ceramics before and after annealing and quenching.
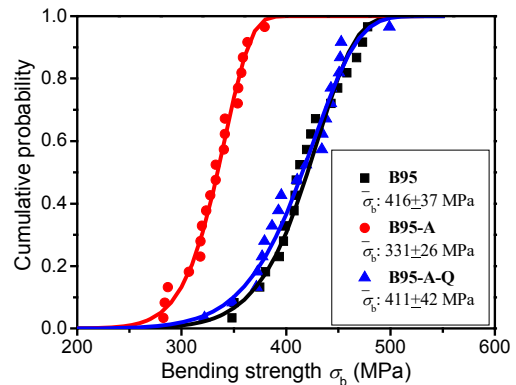

Fig. 6 Measured bending strength σ_b data of B95 samples sorted in ascending order and the Weibull distribution fitting (lines). The inset data $\overline{\sigma}_b$ is the average value of σ_b with the standard deviation.

improved the propagation of the DB channel and reduced the DBS of the 95% alumina ceramics.

However, the shape parameters of the Weibull distribution fitting in the DB test were much higher than the corresponding shape parameters of Weibull distribution fitting in the bending strength measurement, as listed in Table 2, and this difference was also

discovered by Neusel *et al*. [18]. Additionally, the Weibull distribution fitting of the measured bending strength data of B95-A was much better than the Weibull distribution fitting of the measured DBS data of B95-G-A. This can be observed by comparing Fig. 2(c)

Table 2 Shape parameters of the Weibull distribution fitting in the dielectric breakdown test and the bending strength measurement of B95 samples

Sample in dielectric breakdown test	B95-G	B95-G-A	B95-G-A-Q
Shape parameter (95% confidence)	22.63 (16.58–30.88)	23.84 (17.78–31.98)	16.25 (11.62–22.73)
Sample in bending strength measurement	B95	B95-A	B95-A-Q
Shape parameter (95% confidence)	12.64 (9.03–17.72)	14.59 (10.40–20.47)	10.90 (7.84–15.16)

with Fig. 6. As a result, the correlation between the DB and the mechanical fracture is not so simply through the identical defects, but may be attributed to the fact that DB and mechanical fracture are both dependent on the energetics of the mechanically strained lattice [12]. The strained lattice has a higher energy level, and is easier to be broken than the non-strained lattice. In the DB process, when high electric field is applied, the incident electron excites the electrons from the valance band to the conduction band at the strained lattice easier than at the non-strained lattice, so the happening of the avalanche DB is more likely in the alumina ceramics full of strained lattice. Much more attention should be focused on studying this straining mechanism.

The result that the DBS of B95-G-A-Q was higher than the DBS of B95-G may be attributed to the small grains on the surface generated by the coarsening of the fragments as shown in Fig. 4. This is because it was widely found that the DBS of ceramics decreased with the increasing grain size [9,19,24]. Because of tight industrial tolerances, the alumina ceramics which are sealed to metal need to be ground after sintering [25]. High temperature quenching can be used to improve their DBS after the grinding.

It is interesting that annealing improved the DBS of A99. No obvious changes were found in the material characterizations of A99 before and after annealing. The phenomenon could not be attributed to the elimination of defects on the surface, because polishing did not reduce the DBS of A99-AT. More work is needed to find the mechanism behind the effect of annealing on the DBS of A99.

3. 4 Analyses on the underlying mechanisms behind the effects of firing in wet hydrogen

The improvement of firing in wet hydrogen on the DBS of alumina ceramics can be attributed to the reduction in the concentrations of point defects and electrical carriers. DB is always associated with electrical carriers and their transport [26]. At room temperature, the electrical conductivity is dominant in alumina [27]. For

the perfect alumina crystal, the electrical carriers are mainly the electrons in the conduction band and the holes in the valence band that are generated by the thermal excitation. When the electric field is high, space charge limited conduction is the dominant conduction mechanism [28,29]. In the thermal DB theory and the avalanche DB theory, the large current induced by the strong electric field can lead to more excited electrical carriers and subsequently the DB. In the recent Schneider's Griffith type energy release rate model for the DB, the conduction mechanism at the tip of filament is also critical to the DB process [30,31]. The improvement of firing in wet hydrogen on the DBS of alumina ceramics might be associated with the reduction in the concentrations of electrical carriers due to the effects of ambient atmosphere on the chemical equilibria of point defects in the alumina ceramics.

Optical characterization is always used to investigate the point defects in the material. In our experiment, firing in wet hydrogen improved reflectance of the three alumina ceramics in the UV region, as shown in Fig. 7, and the result was consistent with the result of Atlas and Firestone [32]. Firing in wet hydrogen improved the reflectance of the three alumina ceramics in UV region, while it reduced their reflectance in Vis–IR region, making them look darker. Atlas and Firestone [32] attributed the increase in the reflectance in the UV region to the partial elimination of aluminum vacancies. Besides, another proposition is reasonable: the increase in the reflectance in the UV region is attributed to the partial elimination of interstitial oxygen. Lagerlöf and Grimes [33] argued that the interstitial oxygen is the dominant point defect in the pure alumina, and Kozakiewicz *et al*. [34] found that the interstitial oxygen increased the absorbance of alumina in the UV region. In any case, the increase in the reflectance in the UV region indicates the reduction in the concentration of point defects. The reduction in the concentration of point defects inevitably brings the reduction in the concentration of electrical carriers, which reduces the electrical conductivity.

Firing in wet hydrogen indeed reduced the electrical
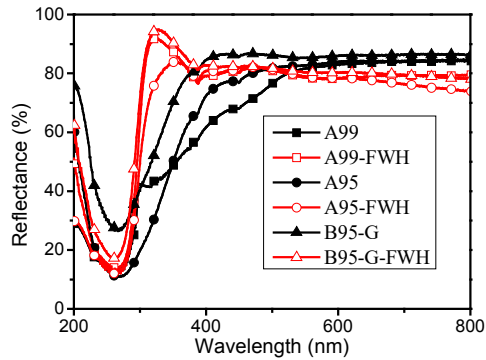
Fig. 7 Reflectance spectra of the alumina ceramics before and after firing in wet hydrogen.

conductivities of A99 and A95 (ESM), and the result was consistent with the result of Pappis and Kingery [10]. The water added into the hydrogen suppressed the generation of electrons (more discussion on the chemical reactions can be found in the ESM). Firing in wet hydrogen improved the DBS of alumina ceramics. On one hand, the alumina ceramics fired in wet hydrogen have a lower concentration of point defects, and under the high electrical field, the concentration of the electrical carriers excited by the incident electrical carriers is lower. On the other hand, the alumina ceramics fired in wet hydrogen have a lower concentration of electrical carriers, and that means the concentration of the incident electrical carriers is lower, leading to a lower concentration of excited electrical carriers under the high electric field. Some other researchers have improved the DBS of inorganic dielectric materials by reducing the concentrations of the point defects. Huang *et al*. [35] improved the DBS of the Al_2O_3–SiO_2–TiO_2 ceramics by doping Ni_2O_3, and they attributed the improvement to inhibiting the oxygen vacancies because of the reaction $1/2Ni_2O_3 \rightarrow NiO + 1/2O_2$. Yao *et al*. [36] improved the DBS of the Al_2O_3 film by doping TiO_2, and they attributed the improvement to the decrease in the oxygen vacancies due to the doping. Much more work on the effect of point defects on the DBS of alumina ceramics is needed.

3. 5   Comparison among the dielectric breakdown strengths of A99-G, A95-G, and B95-G

Generally, the DBS of alumina ceramics decrease with increasing porosities, which explains why A99-G had the highest DBS among the as-sintered and ground samples. This conclusion is reached because the porosities of A99, A95, and B95 were 1.5%, 4.8% and 6.0%, respectively. The porosity is calculated as $1 - \rho/\rho_0$,

where ρ and ρ_0 are the actual density and the theoretical density, respectively, and the actual densities are listed in Table 2. The theoretical density of A99 is 3.98 g/cm^3, and the theoretical density of A95 and B95 is about 3.90 g/cm^3. Nevertheless, different arguments on how much the increasing porosity reduced the DBS of alumina ceramics still exist. Liebault *et al*. [8] reported that the porosities below 5% had no effect on the DBS of ceramics, and Haddour *et al*. [37] reported that porosities had weak influence on the DBS of alumina ceramics beyond 92% densification. However, Neusel *et al*. [18] found that the increasing porosity still strongly reduced the DBS of an alumina ceramic even when it was below 5%. There must be some factors causing the differences among the results obtained by Refs. [8,18,37]. In our experiment, A99-G had a much lower porosity than the 95% alumina ceramics, and the DBS of A99-G was only 8% higher than the DBS of the ground alumina ceramics. However, the difference seems unnoticeable when it is compared with the differences reported by Ref. [18], in which the DBS of the alumina ceramic of 1.8% porosity was 38% higher than the DBS of the alumina ceramic of 6.3% porosity. Besides, the DBS of A95-G was almost equivalent to the DBS of B95-G, although A95-G had a lower porosity. The result in our experiment was more similar to the result of Ref. [37].

In our recent study, it was found that the DBS of alumina ceramics decreased with the increasing of pores in quantities and sizes [38]. In the study of Ref. [37], with the increasing of the addition of rice starch to the raw powder of alumina ceramics, the porosity and the sizes of pores both increased, so the addition of rice starch had a twofold effect on the DBS of alumina ceramics. However, the alumina ceramics investigated in the study of Ref. [37] were all sintered from compacted powder. Pores in alumina ceramics sintered from compacted powder are always small, and this might be the main reason why our result in this study and the result of Ref. [37] were different from the result of Ref. [18].

4   Conclusions

In this study, effects of annealing and firing in wet hydrogen on the DBS of three alumina ceramics were studied. Annealing decreased the DBS of the 95% alumina ceramics, and improved the DBS of the 99%

alumina ceramic. Firing in wet hydrogen improved the DBS of alumina ceramics. The DBS data of the annealed 95% alumina ceramics cannot be fitted to the Weibull distribution well, and this was different from the previous reports.

The inter-granular phase crystallization that reduced the DBS of the 95% alumina ceramics after annealing, and the micro-cracks generated by the mismatch between the alumina matrix and crystalline inter-granular phases can be used to explain the phenomenon that was proven by the measurement of bending strengths. However, the correlation between the DB and the mechanical fracture is not so simply through the identical defects such as the microcracks, and this argument was convincingly demonstrated by the comparison between the Weibull distribution fitting in the DB test and the Weibull distribution fitting in the bending strength measurement. No obvious changes were found in the material characterizations of A99 before and after annealing.

For the ground 95% alumina ceramic, the DBS of the quenched samples was higher than the DBS of as-sintered samples, and the improvement due to quenching on the DBS may be attributed to small grains on the surface generated by the coarsening of fragments.

The improvement of firing in wet hydrogen on the DBS of alumina ceramics can be attributed to the reduction in the concentrations of point defects and electrical carriers, which was convincingly demonstrated by the measurement of reflectance spectra and electrical conductivities.

Electronic Supplementary Material

Supplementary material is available in the online version of this article at https://doi.org/10.1007/s40145-019-0357-x.

References

[1]   Carter CB, Norton MG. *Ceramic Materials*. New York, USA: Springer New York, 2013.

[2]   Park CW, Yoon DY. Effects of SiO_2, CaO_2, and MgO additions on the grain growth of alumina. *J Am Ceram Soc* 2004, **83**: 2605–2609.

[3]   Baik S, White CL. Anisotropic calcium segregation to the surface of Al_2O_3. *J Am Ceram Soc* 1987, **70**: 682–688.

[4]   Frueh T, Marker C, Kupp ER, *et al*. Powder chemistry effects on the sintering of MgO-doped specialty Al_2O_3. *J Am Ceram Soc* 2018, **101**: 2739–2751.

[5]   Powell-Dogan CA, Heuer AH. Microstructure of 96% alumina ceramics: I, characterization of the as-sintered materials. *J Am Ceram Soc* 1990, **73**: 3670–3676.

[6]   Powell-Dogan CA, Heuer AH. Microstructure of 96% alumina ceramics: II, crystallization of high-magnesia boundary glasses. *J Am Ceram Soc* 1990, **73**: 3677–3683.

[7]   Powell-Dogan CA, Heuer AH. Microstructure of 96% alumina ceramics: III, crystallization of high-calcia boundary glasses. *J Am Ceram Soc* 1990, **73**: 3684–3691.

[8]   Liebault J, Vallayer J, Goeuriot D, *et al*. How the trapping of charges can explain the dielectric breakdown performance of alumina ceramics. *J Eur Ceram Soc* 2001, **21**: 389–397.

[9]   Touzin M, Goeuriot D, Guerret-Piécourt C, *et al*. Alumina based ceramics for high-voltage insulation. *J Eur Ceram Soc* 2010, **30**: 805–817.

[10]   Pappis J, Kingery WD. Electrical properties of single-crystal and polycrystalline alumina at high temperatures. *J Am Ceram Soc* 1961, **44**: 459–464.

[11]   Miranzo P, Tabernero L, Moya JS, *et al*. Effect of sintering atmosphere on the densification and electrical properties of alumina. *J Am Ceram Soc* 1990, **73**: 2119–2121.

[12]   Damamme G, Le Gressus C, de Reggi AS. Space charge characterization for the 21th century. *IEEE Trans Dielect Electr Insul* 1997, **4**: 558–584.

[13]   Jaitly N, Sudarshan T, Dougal R, *et al*. Degradation due to wet hydrogen firing on the high-voltage performance of alumina insulators in vacuum applications. *IEEE Trans Elect Insul* 1987, **EI-22**: 447–452.

[14]   Medvedovski E, Peltsman M. Low pressure injection moulding mass production technology of complex shape advanced ceramic components. *Adv Appl Ceram* 2012, **111**: 333–344.

[15]   Gorjan L, Dakskobler A, Kosmač T. Strength evolution of injection-molded ceramic parts during wick-debinding. *J Am Ceram Soc* 2012, **95**: 188–193.

[16]   ASTM D149-97a(2004). Test method for dielectric breakdown voltage and dielectric strength of solid electrical insulating materials at commercial power frequencies. ASTM International. DOI 10.1520/d0149-97ar04.

[17]   Block B, Kim Y, Shetty DK. Dielectric breakdown of polycrystalline alumina: A weakest-link failure analysis. *J Am Ceram Soc* 2013, **96**: 3430–3439.

[18]   Neusel C, Jelitto H, Schmidt D, *et al*. Thickness-dependence of the breakdown strength: Analysis of the dielectric and mechanical failure. *J Eur Ceram Soc* 2015, **35**: 113–123.

[19]   Carabajar S, Olagnon C, Fantozzi G, *et al*. Relations

between electrical breakdown field and mechanical properties of ceramics. In Proceedings of 1995 Conference on Electrical Insulation and Dielectric Phenomena, Virginia Beach, VA, USA, 1995: 278–281.

[20] Malec D, Bley V, Talbi F, *et al*. Contribution to the understanding of the relationship between mechanical and dielectric strengths of Alumina. *J Eur Ceram Soc* 2010, **30**: 3117–3123.

[21] Tomaszewski H. Effect of the intergranular phase structure on the thermomechanical properties of alumina ceramics. *Ceram Int* 1988, **14**: 93–99.

[22] Padture NP, Chan HM. Improved flaw tolerance in alumina containing 1 vol% anorthite via crystallization of the intergranular glass. *J Am Ceram Soc* 1992, **75**: 1870–1875.

[23] Jouini Z, Malec D, Valdez-Nava Z. Effect of mechanical prestress on the dielectric strength of alumina. In Proceedings of the 2016 IEEE International Conference on Dielectrics (ICD), Montpellier, France, 2016.

[24] Beauchamp EK. Effect of microstructure on pulse electrical strength of MgO. *J Am Ceram Soc* 1971, **54**: 484–487.

[25] German RM, Suri P, Park SJ. Review: liquid phase sintering. *J Mater Sci* 2009, **44**: 1–39.

[26] Blaise G. Charge localization and transport in disordered dielectric materials. *J Electrost* 2001, **50**: 69–89.

[27] Will FG, de Lorenzi HG, Janora KH. Conduction mechanism of single-crystal alumina. *J Am Ceram Soc* 1992, **75**: 295–304.

[28] Talbi F, Lalam F, Malec D. DC conduction of Al_2O_3 under high electric field. *J Phys D: Appl Phys* 2007, **40**: 3803–3806.

[29] Neusel C, Jelitto H, Schneider GA. Electrical conduction mechanism in bulk ceramic insulators at high voltages until dielectric breakdown. *J Appl Phys* 2015, **117**: 154902.

[30] Schneider GA. A Griffith type energy release rate model for dielectric breakdown under space charge limited conductivity. *J Mech Phys Solids* 2013, **61**: 78–90.

[31] Fischer PK, Schneider GA. Dielectric breakdown toughness from filament induced dielectric breakdown in borosilicate glass. *J Eur Ceram Soc* 2018, **38**: 4476–4482.

[32] Atlas LM, Firestone RF. Application of thermoluminescence and reflectance methods to study of lattice defects in alumina ceramics. *J Am Ceram Soc* 1960, **43**: 476–483.

[33] Lagerlöf KPD, Grimes RW. The defect chemistry of sapphire (α-Al_2O_3). *Acta Mater* 1998, **46**: 5689–5700.

[34] Kozakiewicz AG, Davidson AT, Derry TE. VUV optical absorption in sapphire crystals following implantation with 100 keV O+, Al+ and Cr+ ions. *Nucl Instruments Methods Phys Res Sect B: Beam Interactions Mater Atoms* 2002, **191**: 582–585.

[35] Huang Y, Chen Y, Li X, *et al*. Enhanced dielectric breakdown strength in Ni_2O_3 modified Al_2O_3-SiO_2-TiO_2 based dielectric ceramics. *J Eur Ceram Soc* 2018, **38**: 3861–3866.

[36] Yao MW, Xiao RH, Peng Y, *et al*. The influence of titanium doping on the electric properties of amorphous alumina films prepared by sol–gel technology. *J Sol-Gel Sci Technol* 2015, **74**: 39–44.

[37] Haddour L, Mesrati N, Goeuriot D, *et al*. Relationships between microstructure, mechanical and dielectric properties of different alumina materials. *J Eur Ceram Soc* 2009, **29**: 2747–2756.

[38] Zhang T, Lei YJ, Yin J, *et al*. Effects of pores on dielectric breakdown of alumina ceramics under AC electric field. *Ceram Int* 2019, **45**: 13951–13957.